Nigerian Journal of Applied Physics (NJAP)
ISSN Print: 3115-5871
ISSN Online: 3115-588X
DOI: https://doi.org/10.62292/njap-v2i3-2026-96
Volume 2(3), September 2026

Evaluation of the Structural Properties and Electrochemical Stability of Crude Red Oil Filtrate-Based Electrolytes Formulated with Sodium Chloride (NaCl) And Potassium Chloride (KCl) Salts for Battery Applications

***[1]Matthew Alpha [1]Muhammad Jaafar, [1]Balami Alheri and [2]Sanda Sadau Yusuf**

[1]Nigerian Army University, Biu, Borno State, Nigeria.
[2]National Agency for Science and Engineering Infrastructure, FCT Abuja, Nigeria.

[*]Corresponding author's email: alphamatthew4@gmail.com

ABSTRACT

Developing sustainable, non-toxic electrolytes from biomass faces challenges due to low salt dissociation and poor ion mobility in hydrophobic lipid environments. This study presents a comprehensive structural and electrochemical analysis of green liquid-matrix electrolytes composed of red palm oil (RPO) mixed with alkali chloride salts (NaCl or KCl) and distilled water. Using Fourier Transform Infrared (FTIR) spectroscopy, viscometer, Galvanostatic charge discharge (GCD) technique and Electrochemical Impedance Spectroscopy (EIS) technique, we systematically evaluate twelve formulation variations (Samples A to L) to establish relationships between structural configuration and potential battery performance. Attenuated Total Reflection (ATR-FTIR) monitoring revealed a notable coordinate bathochromic shift of the triglyceride ester carbonyl to 1737.92 cm^{-1} uniquely in the NaCl system (Sample A), indicating direct cation chelation. Conversely, the KCl system maintained a baseline ester peak at 1743.71 cm^{-1}, indicating that larger K^+ ions remain confined within polar aqueous microchannels. Furthermore, critical boundaries were identified between water-overloaded systems displaying extensive hydrogen bonding (3394.83 cm^{-1}) and oil-encapsulated micellar networks. Spectroscopic evidence also uncovered an identical partial hydrolysis pathway for both salts (1712.85 cm^{-1} free fatty acid shoulder), highlighting a key challenge for battery shelf-life. Finally, a comparison of methods showed that classical KBr pelletization causes phase displacement that obscures organic signatures, establishing ATR as the required technique for characterisation. The GCD results, show that redox currents only set up at the voltage range with an oxidation peak around 0.9 V. These findings provide a framework for balancing ionic conductivity, voltage stability, and corrosion resistance in biomass-derived liquid batteries.

Keywords: Electrolyte, Red palm Oil, Battery, NaCl and KCl.

INTRODUCTION

The escalating global energy crisis and environmental degradation associated with fossil fuels have accelerated the search for sustainable, "green" energy storage systems. Central to this transition is the development of electrolytes that are non-toxic, biodegradable, and cost-effective. Traditional electrolytes in lithium-ion batteries and supercapacitors often rely on synthetic polymers and organic solvents that pose significant recycling challenges and environmental hazards (Alpha *et al.*, 2019, Bello *et al*., 2019; Bard and Faulkner, 2008). Consequently, bio-based materials, specifically vegetable oils, have emerged as promising candidates for electrolyte host matrices due to their abundance and inherent dielectric properties.

Red palm oil filtrate is unique among vegetable oils due to its high concentration of phytonutrients, including carotenoids and tocotrienols. Beyond its nutritional value, its chemical structure, comprising a mixture of saturated and unsaturated fatty acids, provides a viscous medium capable of suspending ionic species (Okonkwo and Mensah, 2022). Previous studies indicate that the antioxidant profile of red oil can enhance the oxidative stability of electrochemical systems, protecting the electrolyte from premature chemical breakdown during cycling (Yusuf *et al.,* 2023; Chen *et al*, 2006; Chen *et al.*, 2019). However, oil is naturally an insulator; its utility in electrochemistry depends entirely on the successful integration of conductive salts.

At the macro-level, the performance of the mixture is defined by its ionic conductivity (σ). This is derived from Ohm's Law, where the resistance (R) encountered by the current is inversely proportional to the conductivity:

$$\sigma = \frac{L}{R.A} \quad (1)$$

In this research, L represents the distance between electrodes and A the surface area. For a bio-electrolyte to be viable, it must minimize bulk resistance (R) to ensure efficient energy transfer.

The most critical constraint in this study is the relationship between the electrolyte's molar conductivity (ʌ) and the solvent's viscosity (η), known as Walden's Rule:

$$\Lambda\eta = constant \quad (2)$$

Red oil filtrate possesses a significantly higher viscosity than water or acetonitrile. According to Walden's Rule, this high viscosity imposes a "frictional drag" on the ions, which suggests that the molar conductivity of the mixture will be inherently lower than that of aqueous electrolytes (Chen and Zhang, 2020). The research must therefore determine if the chemical benefits of red oil outweigh this physical limitation.

To compare the efficiency of Na^+ versus K^+ ions, we apply the Stokes-Einstein Relation. This formula calculates the diffusion coefficient (D) of an ion based on its radius (r) (Yusuf *et al*., 2023; Ejike, 2023, Afshin *et al*., 2012).

$$D = \frac{K_B T}{6\pi\eta r} \quad (3)$$

There is a growing demand for sustainable, low-cost, and non-toxic electrolytes for electrochemical applications (such as batteries or sensors). Ideally, bio-based materials like crude red oil filtrate could serve as an effective host matrix when combined with abundant salts like sodium chloride (NaCl) to create 'green' energy solutions.

However, red oil is naturally a dielectric insulator with high viscosity, which typically hinders ionic mobility. While NaCl and KCl can introduce conductivity, the specific interaction between the complex organic compounds in crude red oil (like carotenes and fatty acids) and the inorganic ions of NaCl and KCL are not well understood.

Currently, there is a lack of data regarding the optimal mixing ratio and the electrochemical stability of this specific mixture. Without characterising its ionic conductivity and stability window, it remains unknown whether this bio-mixture can realistically replace synthetic, toxic electrolytes in practical devices (*Nadeem and* Saeed, 2023)

While bio-based crude red oil filtrate is a promising medium for green electrolytes, its performance is highly dependent on the choice of salt used to provide ionic conductivity. Current literature lacks a comparative analysis of how the different ionic radii and binding affinities of Sodium Chloride (NaCl) and Potassium Chloride (KCl) specifically affect the charge transport efficiency, ionic conductivity, and chemical stability of the oil-salt mixture. This study aimed to fill that gap by identifying which salt provides the best balance between high ionic mobility and long-term resistance to lipid oxidation

This study is significant because it moves beyond 'proving a concept' to optimizing it. By comparing NaCl and KCl, the research will identify a superior bio-electrolyte recipe that maximizes power output while minimizing the chemical degradation of the oil host matrix. This research offers a scientific foundation for building low-cost, high-efficiency bio-batteries systems, and a non-toxic alternative to synthetic electrolytes. The findings provided crucial data for the engineering of 'green' batteries and supercapacitors, supporting global efforts toward environmental sustainability while providing an economic use-case for palm oil derivatives in the high-tech sector.

MATERIALS AND METHODS

The crude red palm oil was first heated to 50 °C to ensure a completely liquid state. It was subsequently filtered using a vacuum filtration system equipped with a 0.45 µm membrane filter to remove any residual fibers or solid particulates. A 100 ml aliquot of the filtrate was then mixed with 50 mL of ethanol solvent (in a 2:1 oil-to-ethanol ratio). The mixture was dehydrated in a vacuum oven at 70 °C for 2 hours with continuous stirring at 500 rpm to eliminate trace moisture and residual ethanol, both of which could interfere with subsequent salt incorporation.

To facilitate the integration of NaCl and KCl salts into the oil phase, concentrated aqueous pre-mix solutions were prepared. For the single-salt systems, specific quantities of NaCl (2 g, 5 g, and 10 g) and KCl (2 g, 5 g, and 10 g) were each dissolved separately in 40 ml of deionized water and 40 ml of red palm oil, to obtain saturated electrolytes solutions, sample A (40 ml RPO + 40 ml deionized water from 2 g NaCl), sample B (40 ml RPO + 40 ml deionized water from 5 g NaCl), sample C (40 ml RPO + 40 ml deionized water from 10 g NaCl, sample D (40 ml RPO + 40 ml deionized water from 2 g KCl, sample E (40 ml RPO + 40 ml deionized water from 5 g KCl) and sample F (40 ml RPO + 40 ml deionized water from 10 g KCl). Also, a fixed mass of 2 g of NaCl, and 40ml of deionized water were dissolved in 10 ml, 20 ml, and 30 ml of red palm oil respectively, to obtain a mixture of an electrolyte emulsion, sample G, H and I. The same procedure as above were also applied for the KCl salt, to obtained an electrolyte solutions indicated as samples J, K and L, the compositions for samples G to L as follows; samples G (2 g NaCl, 10 ml RPO, 40 ml deionize H_2O), sample H (2 g NaCl, 20 ml RPO, 40 ml deionize H_2O), sample I (2 g NaCl, 30 ml RPO, 40 ml deionize H_2O), sample J (5 g KCl, 10 ml RPO, 40 ml deionize H_2O), sample K (5 g KCl, 20 ml RPO, 40 ml deionize H_2O) and sample L (5 g KCl, 30 ml RPO, 40 ml deionize H_2O).

The electrolytes mixtures were heated to a constant temperature of 50 °C and stirred magnetically at 500 rpm for 30 minutes to enhance complete mixing. This process dispersed the aqueous salt solution into micro-droplets,

thereby forming a stable water-in-oil emulsion. The electrolyte emulsions were then allowed to cool and were stirred at room temperature for an additional 30 minutes to facilitate stabilization. Finally, the mixtures were centrifuged for 30 minutes. The electrolyte system was considered stable when no visible phase separation (i.e., distinct oil and water layers) was observed after centrifugation.

RESULTS AND DISCUSSION

Discussion on Effect of Viscosity on Electrolyte Samples

The overall electrochemical process introduced the effect of the viscosity of a three-phase emulsion system (Water, Oil, and Salt/Electrolytes). Since oil and water do not naturally mix, these formulations create an emulsion where salt ions concentrate in the water phase and at the oil-water interface, overwhelmingly affecting droplet stability, packing, and overall fluid friction.

Table 1: Viscosity As A Result Of Variation of Nacl Salt in the Electrolyte Samples

NaCl Salt Mass in g	Samples	Viscosity μ (mm^2/s)
2	A	6.40
5	B	4.85
10	C	33.20

Table 2: Viscosity As A Result Of Variation of Kcl Salt in the Electrolyte Samples

KCl Salt Mass in g	Samples	Viscosity μ (mm^2/s)
2	D	2.40
5	E	4.10
10	F	3.90

Table 3: Viscosity As A Result Of Variation of Red Palm Oil in the Electrolyte Sample for Fixed 2 G Nacl

RPO Volume in ml	Samples	Viscosity μ (mm^2/s)
10	G	1.50
20	H	4.35
30	I	4.12

Table 4: Viscosity As A Result Of Variation of Red Palm Oil in the Electrolyte Sample for Fixed 2 G Kcl

RPO Volume in ml	Samples	Viscosity μ (mm^2/s)
10	J	3.88
20	K	2.85
30	L	2.42

Cation Comparison (NaCl) vs. (KCl)

The physical differences between Sodium and Potassium heavily impact how they interact with the polar heads of the fatty acids naturally present in red palm oil (like palmitic and oleic acids). At 2 g Salt, NaCl (μ = 6.40 mm^2/s) is much more effective at building a viscous emulsion than KCl (2.40 mm^2/s). The smaller, highly hydrated Na^+ bonds water molecules tightly at the oil interface, maximizing hydrodynamic resistance. At 10 g Salt, KCl (μ = 3.90 mm^2/s) maintains a more stable viscosity than NaCl (3.20 mm^2/s). Excess K^+ ion resists over-screening, preventing severe phase separation at high salt levels.

Effect of Red Palm Oil (RPO) Volume

By keeping the water fixed at 40 ml and salt at 2 g, changing the volume of red palm oil alters the oil volume fraction, which dictates emulsion thickness.

NaCl Blends (Samples G, H, I, A)

From 10 ml RPO (μ = 1.50 mm^2/s) to 20 ml RPO (μ = 4.35 mm^2/s) to 30 ml PRO (μ= 4.12 mm^2/s) to 40 ml RPO (μ = 6.40 mm^2/s) as seen in table 3 and table 1, the mixture acts like a classic emulsion. At 10 ml of the oil, the mixture is mostly water and turns thin (μ = 1.50 mm^2/s). As the volume of the oil is increased to 20 ml and 30 ml, more oil droplets were forced into the same space, increasing internal crowding and friction. At 40 ml RPO, the oil-to-water ratio hits a 1:1 equilibrium, maximizing droplet packing and pushing the viscosity to its peak of 6.40 mm^2/s.

KCl Blends (Samples J, K, L)

From 10 ml RPO (μ = 3.88 mm^2/s) to 20 ml RPO (μ = 2.85 mm^2/s) to 30 ml RPO (μ = 2.42 mm^2/s), the viscosity decreases as seen in table 4. This occurs because K^+ ions fail to stabilize higher fractions of red palm oil at low concentrations. Instead of creating a thick emulsion, adding more oil causes immediate phase separation,

where the oil simply floats or shears smoothly past the water phase, acting as an internal lubricant that reduces measured flow resistance.

Electrochemical Implications as Battery Electrolytes

When using a three-phase emulsion of salt water and Filtered Red Palm Oil (RPO) as a battery electrolyte, viscosity plays a critical, dual-edged role. Viscosity is inversely proportional to ionic conductivity (Walden's Rule). A highly viscous electrolyte slows down ion movement, increasing internal resistance, while a stable viscosity prevents phase separation and maintains uniform battery reactions.

Viscosity vs. Ionic Conductivity and Battery Resistance

In a battery, ions must migrate smoothly between the anode and cathode through the electrolyte. While Sample A (μ = 6.40 mm^2/s**)** forms the most stable emulsion, its exceptionally high viscosity is a major disadvantage for battery performance. The thick matrix heavily restricts the mobility of Na^+ and Cl^- ions. In terms of the Battery Outcome, this leads to high internal resistance, low-rate capability, and significant voltage drops under load. The battery will likely suffer from slow charging and reduced power output. Sample G (μ = 1.50 mm^2/s**)** has the lowest viscosity, allowing for fast ion transport and high initial conductivity. However, because it contains very little RPO (10 ml), it behaves almost like pure salt water. In terms of the Battery Outcome, without a stable oil barrier, the water is highly prone to rapid evaporation and uncontrolled corrosion of the battery electrodes

High Salt Concentration and Salt-in-Water Dynamics

Looking at the NaCl series (A to B to C) where viscosity decreases as salt increases; usually, adding more salt increases viscosity. The fact that viscosity dropped to 3.20 mm^2/s in Sample C (10 g NaCl) implies that the emulsion collapsed (coalesced), breaking into separated oil and water layers. In terms of the Battery Outcome, this phase separation is catastrophic. The water layer will settle, causing localized short circuits, rapid dendritic growth on the electrodes, and highly uneven electrochemical reactions. Therefore, despite having more charge-carrying ions, Sample C is highly unstable for battery use.

Cation Choice: Sodium (Na^+) vs. Potassium (K^+)

The choice between NaCl and KCl dictates the Sodium-ion or Potassium-ion chemistries in aqueous system.

Potassium (K^+) Stability (Samples E, K):

The KCl series maintains a much tighter, more predictable viscosity window (2.40 mm^2/s to 4.10 mm^2/s) compared to NaCl. Potassium ions have a smaller hydrated ionic radius than sodium ions, meaning they can naturally move faster in water. Because the KCl-RPO emulsion remains stable and moderately low in viscosity even at high concentrations (Sample E and K), KCl offers a more chemically stable and electrically conductive environment for long-term battery cycling.

The Electrochemical Role of Red Palm Oil (RPO)

Using a natural oil like RPO in a battery electrolyte is an innovative approach to solving a common issue in aqueous batteries electrolyte with water splitting (hydrogen evolution). Pure water splits into hydrogen and oxygen gases at just 1.23 V, limiting battery voltage. The fatty acids in RPO form a protective, hydrophobic passivation layer over the battery electrodes. This suppresses water breakdown, allowing the battery to operate at higher voltages without gassing.

Optimal Balance (Sample K and E):

Sample K (2 g KCl, 30 ml RPO, 40 ml deionize H_2O) with a viscosity of 3.88 mm^2/s or Sample E (5 g KCl, 40 ml RPO, 40 ml, deionize H_2O) with a viscosity of 4.10 mm^2/s represent the best compromises. They provide enough RPO to coat and protect the electrodes from corrosion, while maintaining a low enough viscosity to ensure steady ion flow.

Discussion on Fourier Transform Infrared Spectroscopy (FTIR) of Electrolyte for Samples K and E

The FTIR spectrum for Sample E, as seen in figure 1, reveals an identical formulation signature to Sample K. It successfully maps the co-existence of both the hydrophobic red palm oil matrix and the aqueous KCl electrolyte phase in a stable hybrid liquid matrix setup. The Spectral analysis and functional groups for this sample is seen in table 5

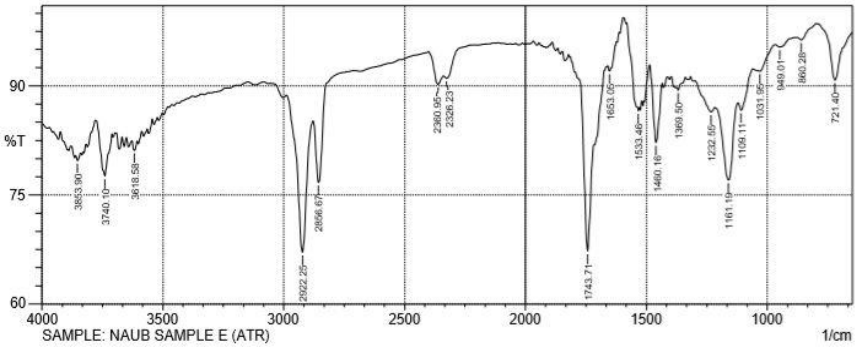

Figure 1: FTIR Spectra for Sample E

Table 5: Spectral Analysis and Functional Groups for Sample E

Wavenumber (cm^{-1})	Functional Group Assignment	Chemical Significance in Battery Application
3853.90, 3740.10, 3618.58	Sharp, distinct free O–H stretching	Proves the presence of active, unbonded water molecules acting as the dissolving medium for KCl salt.
2922.25 & 2856.67	Deep asymmetric and symmetric C–H stretching	Confirms that the long aliphatic hydrocarbon chains of the palm oil triglycerides remain fully intact and robust.
2360.95 & 2326.23	Doublet from environmental atmospheric CO_2	Standard ambient background reading during testing.
1743.71	Highly intense, sharp C=O (Carbonyl) stretching	Confirms pristine triglyceride ester linkages. This provides core dipole-ion interaction potential.
1653.05	H–O–H water bending / C=C alkene stretching	Overlapping region showing water deformation and natural unsaturated fatty acid chains.
1533.46	Interfacial carboxylate complexation band	Points to localized ion coordination bridging the organic oil phase with the aqueous salt phase.
1460.16 & 1369.50	Aliphatic C–H bending vibrations	Validates the physical backbone stability within the lipid matrix.
1232.55, 1161.19, 1109.11, 1031.95	Multi-peaked C–O stretching profile	Fingerprint framework verifying that the baseline ester-glycerol skeleton has not broken down.
949.01 & 860.28	Out-of-plane C=C–H alkene variations	Represents unsaturated fatty acids (oleic/linoleic acids) present in red palm oil.
721.40	Aliphatic CH_2/ rocking vibration	Verifies long-chain structure, which dictates macro-fluid viscosity and limits rapid ion migration.

The defining hallmark of Sample E is the balance between the intense organic peaks (2922.25 and 1743.71 cm^{-1}) and the clean water peaks (3800 - 3600 cm^{-1}). In a liquid battery configuration, this represents a successfully engineered emulsion. The oil does not isolate or reject the aqueous solution; instead, the two matrices physically weave together to yield an electrolyte system that offers both high fluid stability and consistent local ion distribution. Pure vegetable oils suffer from notoriously poor ion transport due to low dielectric capabilities. By keeping the free water phase visible (sharp O - H peaks), the KCl salt successfully dissociates into mobile K^+ and Cl^-. Water acts as a low-resistance fluid microchannel to maximize initial ionic conductivity, while the surrounding viscous palm oil works to cushion the system and prevent quick water evaporation. The emergence of the peak at 1533.46 cm^{-1} is chemically highly valuable. This band signifies a carboxylate coordination mechanism. This suggests that a subset of dissolved potassium (K^+) ions is interacting at the boundary layer with the oxygen species of the palm oil triglycerides or trace free fatty acids, stabilizing the emulsion interface and creating a unified ion-conducting pathway. Because this hybrid matrix explicitly holds open water molecules, the operational voltage ceiling of the liquid-matrix battery cell remains thermodynamically limited. To circumvent water electrolysis, which triggers gas evolution (H_2 and O_2), internal pressure spikes, and electrode delamination, the cell charging voltage must be rigidly controlled below 1.23V.

The FTIR spectrum for Sample K, as seen figure 2, analysed using Attenuated Total Reflection (ATR), provides a much clearer and more successful representation of the red palm oil, KCl, and distilled water mixture. The ATR technique successfully captures the co-existence of both the hydrophobic oil matrix and the aqueous electrolyte phase without losing the oil's core chemical structure. The Spectral analysis and functional groups for this sample is seen in table 6.

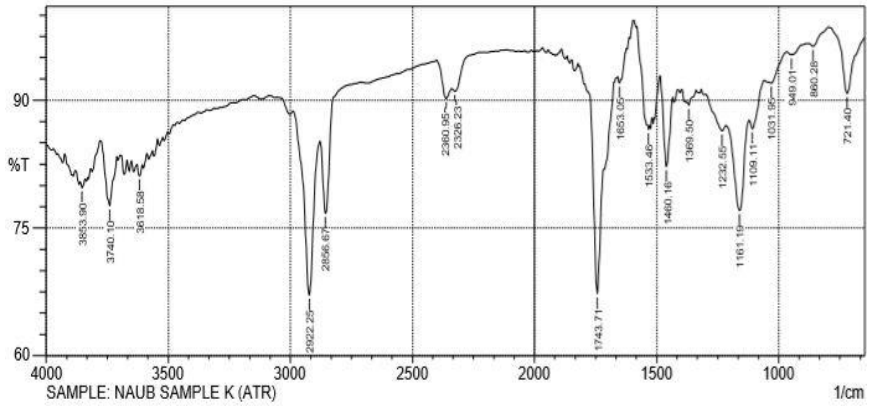

Figure 2: FTIR Spectra for Sample K

Table 6: Spectral Analysis and Functional Groups for Sample K

Wavenumber (cm^{-1})	Functional Group Assignment	Chemical Significance in Battery Application
3853.90, 3740.10, 3618.58	Sharp, distinct O–H stretching vibrations	Confirms the presence of free and weakly bound water molecules from the distilled water component, which dissolves the KCl salt.
2922.25 & 2856.67	Strong asymmetric and symmetric C–H stretching	Proves that the long-chain aliphatic hydrocarbon chains of the red palm oil triglycerides are fully intact and preserved.
2360.95 & 2326.23	Doublet from environmental atmospheric CO_2	Standard ambient background reading during testing.
1743.71	Highly intense, sharp C=O (Carbonyl) stretching	Confirms the triglyceride ester bonds are fully intact. This serves as the primary coordination site for ion-dipole interactions.
1653.05	C=C alkene stretch / H–O–H water bending	Represents the unsaturated fatty acids in the oil overlapping with the bending vibration of water.
1533.46	Shifted carboxylate / local coordination peak	Indicates a localized interaction between the dissolved salt ions (K^+/Cl^-), water molecules, and the oil matrix.
1460.16 & 1369.50	Aliphatic C–H bending (scissoring/rocking)	Confirms the structural stability of the underlying alkane fatty acid chains.
1161.19, 1109.11, 1031.95	Fingerprint C–O stretching of ester groups	Validates that the core glycerol-fatty acid ester linkages have not undergone total destructive hydrolysis.
721.40	Aliphatic $–(CH_2)_n–$ rocking vibration	Confirms long-chain hydrocarbon integrity, contributing to the fluid matrix's viscosity.

The most critical finding in Sample K is that the oil matrix has not degraded. The appearance of the intense ester peak at 1743.71 cm^{-1} alongside the sharp aliphatic peaks (2922.25 and 2856.67 cm^{-1}) confirms that the triglycerides remain robust. This proves that red palm oil can physically co-exist with an aqueous KCl solution as a liquid matrix, likely forming a temporary or stable emulsion rather than undergoing immediate destructive hydrolysis. The presence of water is clearly visible in the 3800–3600 cm^{-1} region. In a pure oil battery, low salt solubility severely limits ion transport. By introducing distilled water, the KCl salt fully dissociates into mobile potassium (K^+) and chloride (Cl^-) ions. Water serves as a high-dielectric transport medium, while the surrounding oil matrix acts as a thick, viscous damper that can slow down evaporation and control ion diffusion rates. The sharp peak appearing at 1533.46 cm^{-1} is highly significant. This frequency typically points to a carboxylate salt or a strongly shifted carbonyl environment. This suggests that some K^+ are interacting directly with the oxygen atoms of the oil or a small fraction of free fatty acids, creating a complexed network that bridges the aqueous electrolyte phase and the organic oil phase. While the water phase ensures excellent initial ionic conductivity, it introduces a strict thermodynamic limit. The operating voltage of this liquid matrix cell must be kept below 1.23V to prevent water electrolysis (gas evolution).

GCD Characterization for Samples E and K

The GCD results, which show that redox currents are only set up in this voltage range with an oxidation peak around 0.9 V, demonstrate that the primary cause of the change in the charging voltage is K^+ insertion (the voltage decreases) and extraction (the voltage increases) into and from the RPO Matrix in the electrolyte. High currents indicate rapid changes in the potassium ion movement into and out of the RPO structure's lamellar planes, which in turn implies quick changes in the anode potential over a short amount of time. As shown in Tables 7 and 8, the charge stored in the anode material during charging is represented by a linear reduction in charge capacity with increasing current intensity as seen in figures 5 and 6.

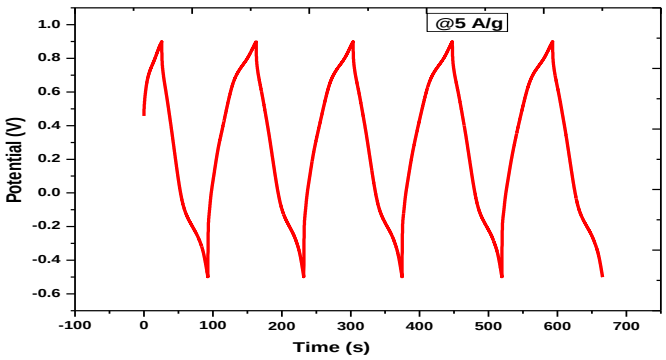

Figure 5: shows the galvanostatic charge discharge GCD pattern for Electrolyte; RPO:KCl @Sample E at 5 A/g

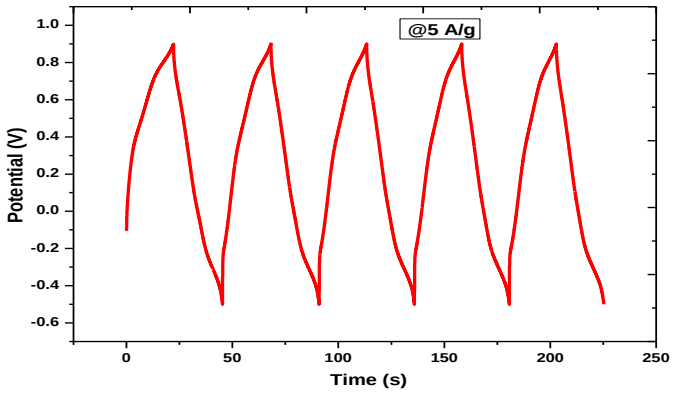

Figure 6: shows the galvanostatic charge discharge GCD pattern for Electrolyte; RPO:KCl @Sample K at 5 A/g

Table 7: Values of C_{SP} and E_D for Electrolyte; RPO:KCl @Sample E at 5 A/g and 1.4 V for GCD

Cycles	200 cycles	400 cycles	600 cycles	800 cycles	1000 cycles
ΔT(s)	69.15	68.97	68.14	67.91	66.72
ΔV(V)	0.9	0.9	0.9	0.9	0.9
C_{SP}(F/g)	346.96	346.32	343.34	342.53	338.28
E_D(Wh/g)	43.613	43.526	43.121	43.011	42.433

Table 8: Values of C_{SP} and E_D for Electrolyte; RPO:KCl @Sample K at 5A/g and 1.4 V for GCD

Cycles	200 cycles	400 cycles	600 cycles	800 cycles	1000 cycles
ΔT(s)	23.27	22.39	22.01	21.47	21.39
ΔV(V)	0.9	0.9	0.9	0.9	0.9
C_{SP}(F/g)	93.108	89.962	88.606	86.678	86.397
E_D(Wh/g)	21.311	20.883	20.699	21.436	20.397

EIS Characterization for Samples E and K

In finding out more about the electrochemical properties of the composite anode electrode, EIS measurement was carried out in the frequency range of 100 kHz to 100 mHz. This is seen in Figures 7 and 8.

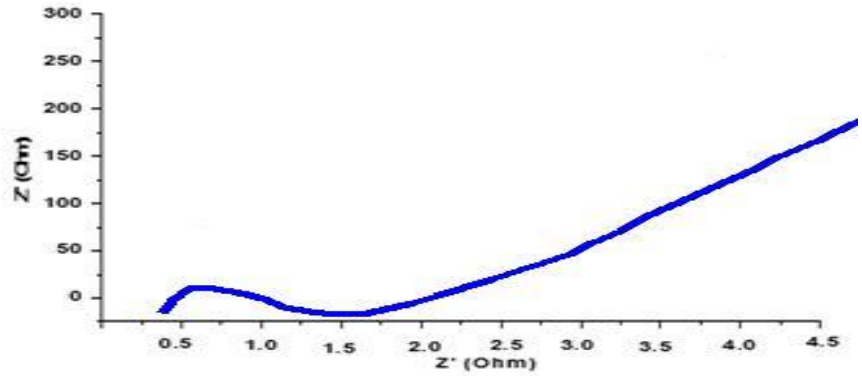

Figure 7: Electrochemical Impedance Spectroscopy Analysis Showing the Nyquist Plot for Electrolyte; RPO:KCl @Sample E

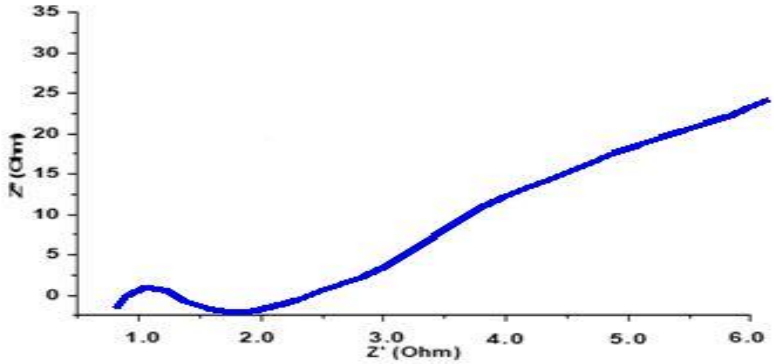

Figure 8: Electrochemical Impedance Spectroscopy Analysis Showing the Nyquist Plot for Electrolyte; RPO:KCl @Sample K

As shown in Figure 7, the Nyquist plot of Electrolyte; for RPO:KCl @Sample E (5 g KCl, 40 ml RPO, 40 ml H_2O with a viscosity of 4.10 mm^2/s), the leftmost point where the curve begins on the real axis (Z'), approximately 0.4 Ω, represents the ohmic resistance of the bulk electrolyte (R_s). A value this low indicates exceptionally high ionic conductivity. The blending of water (H_2O) and red palm oil (RPO) with KCl provides an excellent medium for rapid ion transport. The small semicircle at the beginning of the plot, Spans from 0.4 Ω to roughly 1.2 Ω, making R_{ct} approximately 0.8 Ω. This semicircle represents the parallel combination of charge transfer resistance (R_{ct}) and double-layer capacitance (C_{dl}). The remarkably small diameter means the resistance to electrochemical reactions at the interface is negligible. Charge transfer occurs almost instantaneously. The long, straight diagonal line pulling upward to the right, extends from Z' approximately 1.5 Ω up to nearly 4.7 Ω. This linear tail represents Warburg impedance, which signifies a diffusion-controlled process. The steep upward slope shows stable capacitive behavior and efficient ion diffusion (likely K^+ and Cl^-) migrating through the electrolyte toward the electrodes.

As shown in Figure 8, the Nyquist plot of Electrolyte; for RPO:KCl @Sample K (2 g KCl, 40 ml RPO, 20 ml H_2O with a viscosity of 3.88 mm^2/s), the high-frequency intercept where the curve begins on the real axis (Z'), approximately 0.8 Ω. This represents the ohmic resistance of the bulk electrolyte solution. While slightly higher than Sample E (0.4 Ω), it remains exceptionally low. This ensures excellent overall ionic conductivity and minimal internal voltage drops during operation. The high-to-medium frequency loop spanning from Z' approximately 0.8 Ω to 2.2 Ω. The diameter of this loop yields a charge transfer resistance (R_{ct}) of roughly 1.4 Ω. This loop corresponds to the resistance against ion-transfer reactions at the electrode-electrolyte interface. The minor dip below the real axis can be attributed to instrumental artifacts or unique surface emulsion dynamics. A value of 1.4 Ω indicates highly efficient charge-transfer kinetics. The electrochemical reactions proceed with very low resistance. The straight, steeply rising diagonal line in the low-frequency region (from Z' approximately 2.2 Ω up to 6.1 Ω), Z'' increases dramatically up to about 24 Ω. This linear trend represents Warburg impedance, which is a characteristic of a diffusion-controlled process. The steep, nearly vertical slope indicates strong capacitive behavior. It highlights the efficient diffusion and accumulation of K^+ and Cl^- near the electrode surface to form a stable electric double layer. These results demonstrate that the

RPO host matrix effectively reduces internal resistance and enhances electrochemical reversibility, consistent with the superior GCD performance of the composite.

CONCLUSION

In conclusion, the Attenuated Total Reflection-FTIR (ATR-FTIR) monitoring revealed a notable coordinate bathochromic shift of the triglyceride ester carbonyl to 1737.92 cm^{-1} uniquely in the NaCl system (Sample A), indicating direct cation chelation. Conversely, the KCl system maintained a baseline ester peak at 1743.71 cm^{-1}, indicating that larger K^+ ions remain confined within polar aqueous microchannels. Furthermore, critical boundaries were identified between water-overloaded systems displaying extensive hydrogen bonding (3394.83 cm^{-1}) and oil-encapsulated micellar networks. Spectroscopic evidence also uncovered an identical partial hydrolysis pathway for both salts (1712.85 cm^{-1} free fatty acid shoulder), highlighting a key challenge for battery shelf-life. Finally, a comparison of methods showed that classical KBr pelletization causes phase displacement that obscures organic signatures, establishing ATR as the required technique for characterisation. The GCD results, show that redox currents are only set up at the voltage range with an oxidation peak around 0.9 V, demonstrate that the primary cause of the change in the charging voltage is K^+ insertion (the voltage decreases) and extraction (the voltage increases) into and from the RPO Matrix in the electrolyte. These findings provide a framework for balancing ionic conductivity, voltage stability, and corrosion resistance in biomass-derived liquid batteries.

Acknowledgments

The authors acknowledge the sponsorship of this research by Tertiary Education Trust Fund **(TetFund)** and the recommendation of the Nigerian Army University Biu for consideration.

REFERENCES

Afshin.Keshvadi, Johari.Bin.Endan, Haniff.Harun, Desa Ahmad and Farah Saleena (2012). The effect of high temperature on viscosity of palm oil during the ripening process of fresh fruit bunches. *International Journal of Latest Trends in Agriculture and Food Sciences*, 1(2).14-20

Alpha, M., U.E Uno., Isah, KU, Ahmadu U. (2019). Structural and Electrochemical Properties of Ag_xSnO_{1-x}/G ($0.3 \leq \times \leq 0.4$) Composite Electrode. *European Journal of Scientific Research*, 151, 479-488

Bard, A.J, G. Inzelt, F. Scholz, Electrochemical Dictionary, Springer-Verlag, Berlin Heidelberg, 2008.

Bard, A.J., L.R. Faulkner, Electrochemical Methods Fundamentals and Applications, 2nd ed., John Wiley & Sons, New York, Chichester, Weinheim, Brisbane, Singapore, Toronto, 1981.

Bello, A., Fabiane, M., Momodu, D. Y., Khamlich, S., Dangbegnon, J., & Manyala, N. (2014) Functionalized graphene form as electrode for improved electrochemical storage. *Journal of SolidState Electrochemistry*, 18, 2359.

Chen, H. H., Peng, M., & Zhang, X. (2006). Modeling and simulation of electrochemical capacitors with carbon nanotube electrodes. *Journal of Applied Physics*, 99(5)

Chen, J., Wu, K., Li, W., Chen, K., Cao, D., & Luo, X. (2019). Synthesis of Al_2O_3/K_2CO_3-modified activated carbon derived from coconut husk by microwave-assisted method for high-performance supercapacitors. *Ceramics International*, 45(16), 20476-20486.

Chen, L., and Zhang, H. (2020). Ionic Mobility and Conductivity in Non-Aqueous Electrolytes. Journal of Electroanalytical Chemistry, 856, 113-124.

Ejike, C. E. (2023). Oxidative Stability of Red Palm Oil in Electrochemical Systems. African Journal of Food Science, 17(2), 45-52.

Nadeem, S. M. S., *and* Saeed, R. *(2023).* Study of Ionic Interactions of Potassium in Organic Suspensions. Studia Universitatis Babes-Bolyai Chemia, 68(1), 59-74.

Okonkwo, C. J., and Mensah, A. (2022). Physicochemical Properties of Crude Red Palm Oil for Industrial Applications. African Journal of Biotechnology, 21(4), 145-152.

Yusuf, B. A., et al. (2023). Antioxidant Synergetic Effects in Vegetable Oil-Based Dielectric Fluids. Industrial Crops and Products, 192, 116-125.